



HAL
open science

Effects of the Interaction Length between Hollow Shapes: Application to a HCP Metal under Mechanical Loading

Henri Francillette

► **To cite this version:**

Henri Francillette. Effects of the Interaction Length between Hollow Shapes: Application to a HCP Metal under Mechanical Loading. *Procedia Manufacturing*, 2020, 47, pp.1203 - 1210. 10.1016/j.promfg.2020.04.351 . hal-04059444

HAL Id: hal-04059444

<https://univ-rennes.hal.science/hal-04059444>

Submitted on 5 Apr 2023

HAL is a multi-disciplinary open access archive for the deposit and dissemination of scientific research documents, whether they are published or not. The documents may come from teaching and research institutions in France or abroad, or from public or private research centers.

L'archive ouverte pluridisciplinaire **HAL**, est destinée au dépôt et à la diffusion de documents scientifiques de niveau recherche, publiés ou non, émanant des établissements d'enseignement et de recherche français ou étrangers, des laboratoires publics ou privés.



Distributed under a Creative Commons Attribution - NonCommercial - NoDerivatives 4.0 International License



23rd International Conference on Material Forming (ESAFORM 2020)

Effects of the Interaction Length between Hollow Shapes: Application to a HCP Metal under Mechanical Loading

Henri Francillette*

*Univ Rennes, INSA Rennes, CNRS, ISCR, UMR 6226, 35708 Rennes, France** Corresponding author. Tel.: +33-2-23-23-86-98. E-mail address: henri.francillette@insa-rennes.fr

Abstract

The mechanical response of a hexagonal closed-packed (HCP) metal is analyzed in this study using perforated parallelepiped specimens deformed with a compression device at room temperature in order to generate plastic deformations. Each specimen contains two parallel hollow cylinders for which a characteristic distance d is defined. This length corresponds to the initial length between the two cylinders. Four values of d are considered in the study for specimens cut from a commercially-available pure titanium sheet : $d = 1$ mm, 2 mm, 3 mm and 4 mm. Different experimental characterizations are carried out thanks to the mechanical tests. The experimental force-displacement curves indicate significant level differences for the considered values of d . After the mechanical tests, the geometry of the specimens is analyzed and the microstructures in the vicinities of the new hollow shapes are investigated notably in central, peripheral and upper zones. Different experimental techniques are used for the characterization of the specimens particularly after the mechanical tests, among them electron backscattered diffraction (EBSD).

© 2020 The Authors. Published by Elsevier Ltd.

This is an open access article under the CC BY-NC-ND license (<https://creativecommons.org/licenses/by-nc-nd/4.0/>)
Peer-review under responsibility of the scientific committee of the 23rd International Conference on Material Forming.*Keywords:* Mechanical; Hexagonal; Hollow; EBSD; Twinning

1. Introduction

The study of the mechanical behaviour of hexagonal closed-packed (HCP) metals is particularly important since this class of materials presents several strategic industrial applications. At the same time and from a more fundamental point of view, these metals present strong anisotropic properties during plastic deformation processes. These specific behaviours, which are related to the active deformation modes (slip and twinning), are reported for different pure metals and their alloys, notably for titanium and its alloys [1-4], zirconium alloys [5-7], magnesium alloys [8-9] and zinc alloys [10].

More specifically, titanium and its alloys present particularly strategic applications in the aerospace industry and in the field of medical implants due to respectively high strength to weight ratios, good corrosion resistance and good biocompatibility [11,2,12-14]. Several studies of the literature reveal descriptions of different mechanical tests carried out for commercially pure titanium under different mechanical

loadings. Among them, uni-axial tension or uni-axial compression [1,13-15], cold rolling [16], simple shear [17], equal-channel angular pressing [12,18] and high-pressure torsion [19]. These mechanical tests allow a better understanding of the link between the mechanical properties of the material, the active deformation modes (slip and twinning systems activation) and the geometric and shape changes during forming processes.

Concerning the activation of the deformation modes, several slip and twinning modes are reported in the literature for commercially pure titanium. At room temperature, prismatic glide $\{10\bar{1}0\}\langle 11\bar{2}0\rangle$ is the easiest slip mode whereas basal glide $\{0002\}\langle 11\bar{2}0\rangle$ and first order pyramidal glide of $\{10\bar{1}1\}\langle 11\bar{2}0\rangle$ type and / or $\{10\bar{1}1\}\langle 11\bar{2}3\rangle$ type are the secondary slip modes [1,12,13,15]. For twinning, the frequently activated modes correspond to the extension twins $\{10\bar{1}2\}\langle 10\bar{1}\bar{1}\rangle$ and to the contraction twins $\{11\bar{2}2\}\langle 11\bar{2}\bar{3}\rangle$ [1,13,15,20]. One can notice the ductile behaviour of commercially pure titanium at room temperature. This property

2351-9789 © 2020 The Authors. Published by Elsevier Ltd.

This is an open access article under the CC BY-NC-ND license (<https://creativecommons.org/licenses/by-nc-nd/4.0/>)
Peer-review under responsibility of the scientific committee of the 23rd International Conference on Material Forming.

10.1016/j.promfg.2020.04.351

is particularly interesting when studying the mechanical behaviour of HCP metals. In addition, several experimental techniques, notably electron backscattered diffraction (EBSD), gain access to valuable data at the grain scale in this material.

In this study, the mechanical response of a commercial pure titanium sheet is analysed by considering parallelepiped hollow specimens deformed by applying compressive forces along their normal direction. In the study, d is defined as the distance between two parallel hollow cylinders in each specimen. Four values of d are investigated, notably : 1 mm, 2 mm, 3 mm and 4 mm. The objectives of the study are (i) the determination and the comparison of the force-displacement curves of the different investigated specimens and (ii) the characterization of the geometric changes of the specimens after the mechanical tests (analysis of external and inner surfaces). The objectives are also (iii) the characterization of the microstructures (activation of twinning) in the vicinities of the new hollow shapes of the deformed specimens and (iv) the determination of the crystallographic orientations of grains in particular cases (characterization of twinned and non-twinned parts of grains and local texture determination with pole figures) using EBSD. In the following sections, after the presentation of the experimental procedure, the experimental results with their analysis will be developed before the conclusion.

2. Experimental procedure

In the experimental procedure, parallelepiped specimens are first cut from a received commercial pure titanium sheet with a thickness of 10.7 mm. The chemical composition of the sheet is presented in Table 1. The following initial dimensions are considered for the extracted specimens in the study : $L_0 = 12.0$ mm, $h_0 = 10.7$ mm and $w_0 = 10.0$ mm. L_0 , h_0 and w_0 represent respectively the initial length, height and width of the samples. Then, hollow shapes which correspond to two parallel cylinders of diameter $D = 3$ mm are performed in each specimen with their axes in a parallel position with the width w_0 . The manufacturing technique used to produce the cylinders corresponds to milling. A helical drill (milling cutter) composed of tungsten carbide with a diameter of 2.5 mm has been used to process the hollow shapes. The cylinders are defined also in such a way as their axes are located at the height $h_0/2$ and at the distance a from the external surfaces of area $w_0 \times h_0$ of the samples. The total length of each cylinder corresponds to the width w_0 . Fig. 1 indicates the definition of the characteristic dimensions used for the hollow specimens : d is the length between the two cylinders, L_0 , h_0 and D are already defined. In the study, the samples are cut from the sheet in such a way as L_0 , h_0 and w_0 correspond respectively to the initial rolling direction (RD_0), the initial normal direction (ND_0) and to the initial transverse direction (TD_0) of the sheet. Experimentally, four values of d are considered : 1 mm, 2 mm, 3 mm and 4 mm.

It is worth noting that before the mechanical tests the specimens with their hollow shapes are systematically restored at 800 °C, during 2 hours and under a 10^{-6} mbar vacuum. For the mechanical tests, a 200 kN capacity INSTRON machine is used to carry out the compression of the specimens considering a 1 mm/min cross head speed. The loading direction

corresponds to the height of the specimens. No particular lubricant has been used at the interface between the specimens and the plates of the compression device. All the mechanical tests are carried out at room temperature with strictly the same conditions for each sample, namely with a pre-loading of 50 N followed by a loading time of 140 seconds which is associated with the end of the mechanical test.

Different experimental techniques are used for the characterization of the microstructure of the material. Optical microscopy, with an OLYMPUS PME, is mainly used for characterizing the polycrystalline specimens and for the observation of the active deformation modes after the mechanical tests, notably twinning. At the same time, it is also used for the characterization of the geometric changes of the hollow shapes after the mechanical tests by measuring the variation of characteristic distances defined in the study. A DINO-LITE digital microscope is also used to gain access to macrographs of the deformed specimens. Scanning electron microscopy (SEM) and electron backscattered diffraction (EBSD) are used for the characterization of the microstructures in a JEOL microscope (JSM 7100F) equipped with the OXFORD HKL EBSD system. X-ray diffraction is also used for the validation of the cell parameters of the received commercial sheet. This is a necessary step in the experimental procedure notably for EBSD characterization.

Concerning the surface preparation of the samples for optical observations and EBSD measurements, the specimens are wrapped in a phenolic hot mounting resin with carbon fill for edge retention and examination in SEM. Next, they are mechanically polished with different silicon carbide disks (grades between 380 and 2400) before a final polishing with a non-crystallizing colloidal silica suspension using a STRUERS machine (10 N applied during 45 minutes for each specimen). After these stages, a chemical attack is performed in a solution composed of 1% hydrofluoric acid, 2% of nitric acid and 97% of water, during 30 seconds.

Table 1. Chemical composition of the sheet.

Elements	Ti	Fe	C	N	O	H
Wt %	Remainder	0.03	0.01	<0.01	0.14	0.001

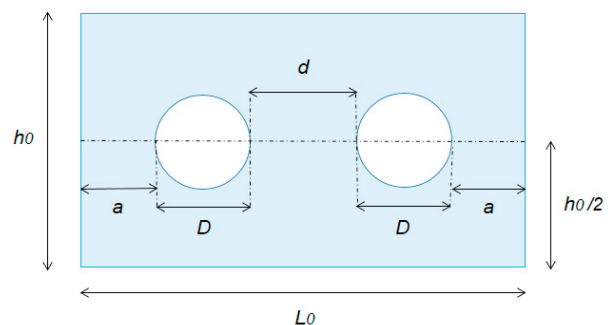


Fig. 1. Geometry of the initial specimens.

Fig. 2 presents the microstructure of the material before the mechanical tests and after the heat treatment at 800 °C. One can notice that the grain boundaries are clearly visible. The grain size is of the order of 80 μm - 100 μm .

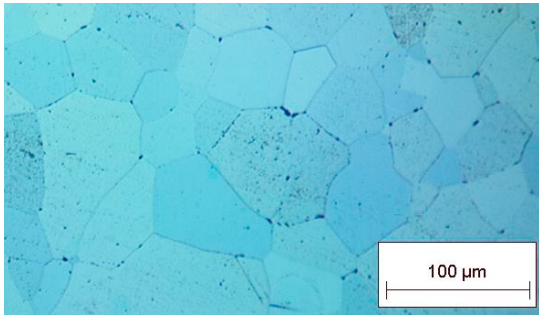


Fig. 2. Initial microstructure of the specimens: (RD_0-ND_0) plane.

3. Results and analysis

Different classes of results are considered in the study and are presented in the following sections. The first section concerns the experimental force-displacement curves which give a first description of the influence of the length d on the mechanical response, thanks to the determination of the force levels and of the shape of the curves. Secondly, the geometry of the specimens is characterized after the mechanical tests. Distances are defined and measured for the external surfaces and for the new hollow shapes that are obtained at the end of the mechanical tests in order to examine geometric variations. In a third part, the microstructures of the samples are characterized in specific zones of the deformed specimens, in the vicinities of the new hollow shapes. Finally, the EBSD technique is used in particular cases in order to gain access to local crystallographic orientations of neighboring grains and to characterize activation of twinning.

3.1. The force-displacement curves

The force-displacement curves are presented in Fig. 3. The comparison of these curves indicates significant differences between them for the force levels and the shapes of the curves.

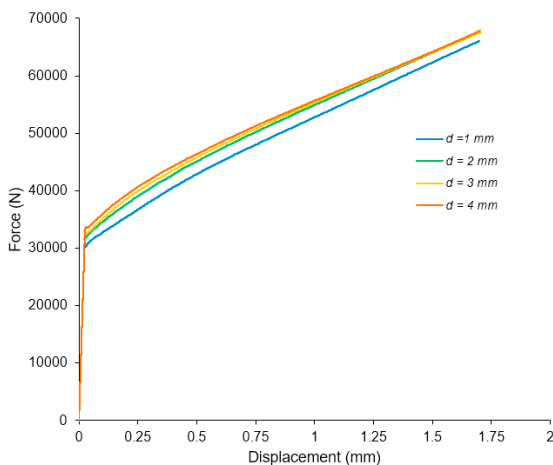


Fig. 3. Experimental force-displacement curves.

The experimental force-displacement curves present a linear part and a non-linear part with specific values of the force at the limit between the two parts : 29880 N for the specimen associated with $d = 1$ mm, 31560 N for $d = 2$ mm, 32760 N for $d = 3$ mm and 33120 N for $d = 4$ mm. For the most part of the non-linear domain, the curves indicate that there is a strict order between them : for a fixed displacement stage, the force level increases when d increases. For instance, at a displacement stage of 0.535 mm, the force equals 42600 N for $d = 1$ mm, 44880 N for $d = 2$ mm, 45720 N for $d = 3$ mm and 45960 N for $d = 4$ mm. The differences between the curves decrease progressively when the displacement increases such that three curves (which correspond to $d = 2$ mm, 3 mm and 4 mm) present similar force levels when the displacement is close to 1.35 mm. The specimen associated with $d = 1$ mm still presents at this displacement stage lower force levels with differences of the order of 2160 N.

Another way to investigate the results is to characterize the geometric variations of the external surfaces and of the hollow shapes at the end of the mechanical tests. This point is considered in the next section.

3.2. Geometry of the specimens after the mechanical tests

The shape changes at a macroscale are presented in Fig. 4 and Fig. 5 for the two specimens associated with $d = 1$ mm and $d = 4$ mm at the end of the mechanical tests.

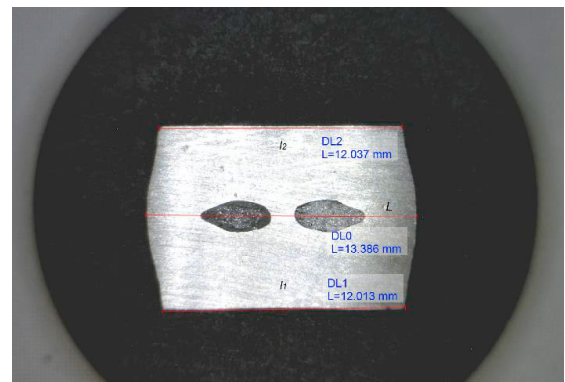


Fig. 4. Macrograph for a small length ($d = 1$ mm).

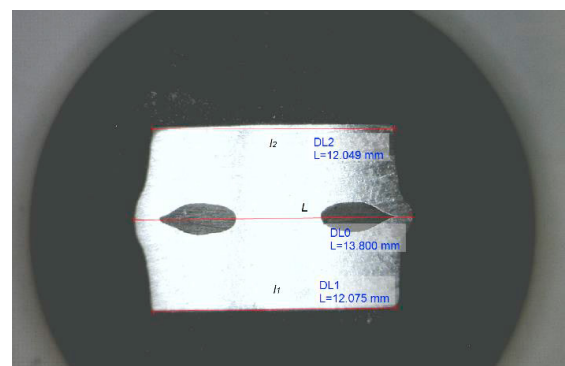


Fig. 5. Macrograph for a large length ($d = 4$ mm).

In the figures, L represents the greater horizontal length of the specimens and l_1 and l_2 represent the horizontal lengths at surface levels (bottom position for index 1 and upper position for index 2). All the experimental values of L , l_1 and l_2 of the investigated specimens are presented in Table 2.

Table 2. Experimental values of the distances L , l_1 and l_2 .

Distances (mm)	L	l_1	l_2
$d = 1$ mm	13.39	12.01	12.04
$d = 2$ mm	13.54	12.08	12.03
$d = 3$ mm	13.68	12.06	
$d = 4$ mm	13.80	12.07	12.05

The comparison of Fig. 4 and Fig. 5 indicates that the curvatures of the external surfaces are different. Moreover, the length L is greater for $d = 4$ mm than for $d = 1$ mm. The evolution of L and l (average value of l_1 and l_2) is presented in Fig. 6 versus d . The evolution of the relative distance variations is also given in Fig. 7 thanks to the knowledge of the initial distances.

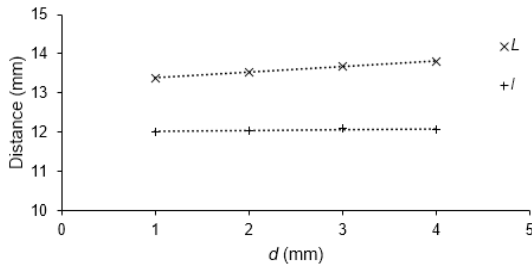


Fig. 6. Evolution of external distances of the deformed specimens.

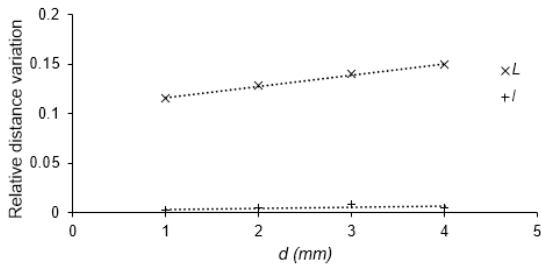


Fig. 7. Relative distance variations of the deformed specimens.

At the end of the mechanical tests, due to the process, new hollow shapes characterize the samples. An illustration of the geometry of such a hollow shape is given in Fig. 8. This figure is associated with the left cylinder of Fig. 1 in the observation plane and is associated with $d = 1$ mm. The dark zone corresponds to the phenolic hot mounting resin with carbon described in the experimental procedure. Here, the size of the new hollow shapes is characterized by the definition of two distances : b the horizontal width and c the vertical height, visible in Fig. 8. The measurements of these distances for the different specimens are presented in Table 3, with index 1 for the shape which appears at the left side in the observation plane and index 2 for the other shape. In Table 3, d^* represents the

experimental value of the length between the two new hollow shapes after each mechanical test.

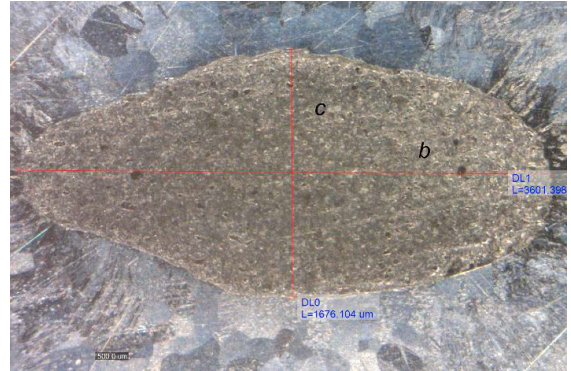


Fig. 8. New hollow shape after the mechanical test ($d = 1$ mm).

Table 3. Experimental values of the distances b_1 , c_1 , b_2 , c_2 and d^* .

Distances (mm)	b_1	c_1	b_2	c_2	d^*
$d = 1$ mm	3.60	1.67	3.54	1.69	1.14
$d = 2$ mm	3.64	1.52	3.63	1.54	2.09
$d = 3$ mm	3.74	1.49	3.74	1.48	3.03
$d = 4$ mm	3.88	1.66	3.70	1.56	4.21

For a more accurate analysis of the values of Table 3, Fig. 9 presents the evolution of the average value noted b of b_1 and b_2 , and the average value noted c of c_1 and c_2 and the value of d^* , versus d .

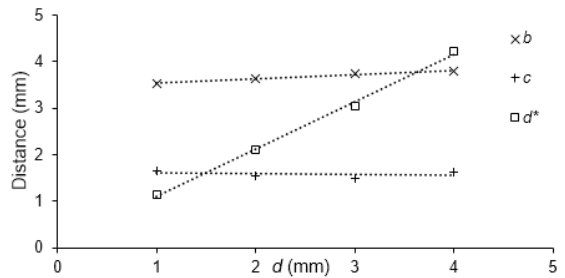


Fig. 9. Evolution of inner distances of the deformed specimens.

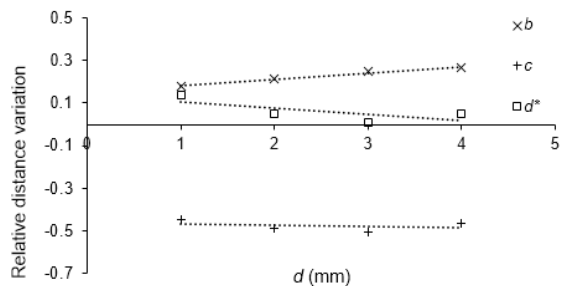


Fig. 10. Relative distance variations of the deformed specimens.

The experimental points indicate linear tendencies for these parameters. From the initial and final experimental dimensions,

the corresponding relative variations are calculated and presented in Fig. 10. The relative distance variations of this figure indicate greater values for b than d^* for a fixed value of d . Reference values in these calculations are the final relative displacement variation associated with the experimental force-displacement curves of Fig. 3 observed at the end of the mechanical tests (close to -0.16) and the values of Fig. 7.

3.3. Microstructures in the vicinity of the new hollow shapes after the mechanical tests

In this part, the microstructures of the deformed specimens are characterized in different areas of the neighbourhood of the new hollow shapes using an optical microscope. (i) Firstly, in the central zone of the samples between the two new shapes, (ii) secondly, in the peripheral zones at the extremities of the hollow shapes, close to the external surfaces of the samples and (iii) finally, in the upper zones above the hollow shapes. The following figures present the results for the lowest and the greatest value of d : 1 mm and 4 mm. The dark areas of the figures correspond as mentioned above to the phenolic resin.

(i) Fig. 11 and Fig. 12 present respectively the first case for $d = 1$ mm and $d = 4$ mm. Fig. 12 represents a partial zone which indicates the location of the hollow shape. The microstructures show activation of twinning. Deformation appears to be significant in the two central zones.

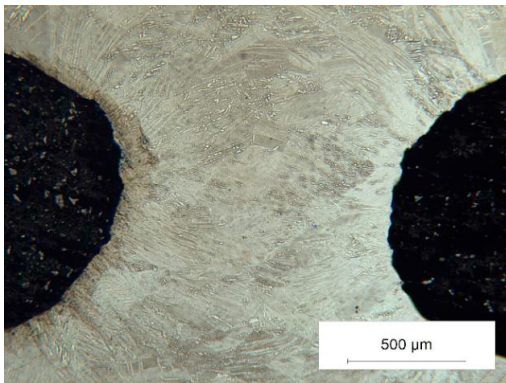


Fig. 11. Central zone for a small length ($d = 1$ mm).

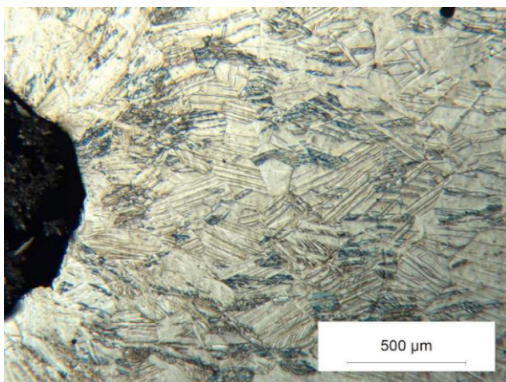


Fig. 12. Central zone for a large length ($d = 4$ mm).

the extremity of the new hollow shapes respectively for $d = 1$ mm and $d = 4$ mm and are associated with left positions in the observation planes. Activation of twinning is visible in both cases. In Fig. 13, this activation is less intensive the further it is situated from the tip of the hollow shape. The local curvature of the external surface can be noted in Fig. 14.

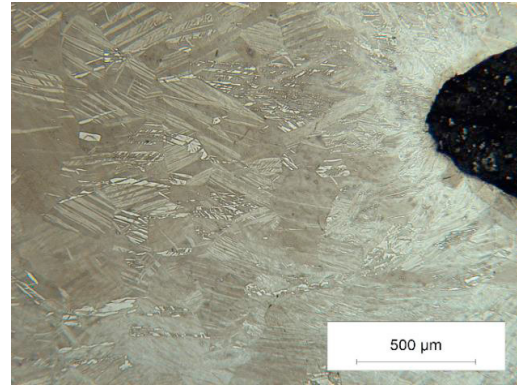


Fig. 13. Peripheral zone for a small length ($d = 1$ mm).

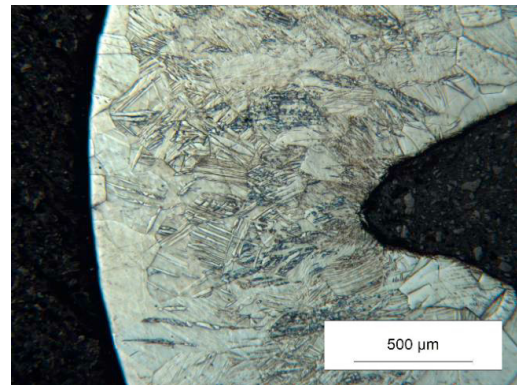


Fig. 14. Peripheral zone for a large length ($d = 4$ mm).

(iii) Fig. 15 and Fig. 16 present the microstructures of the upper zones associated with $d = 1$ mm and $d = 4$ mm, respectively.

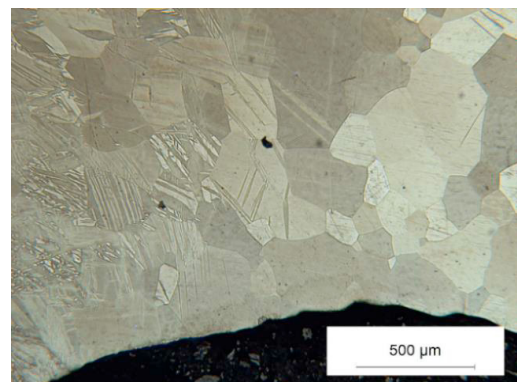


Fig. 15. Upper zone for a small length ($d = 1$ mm).

(ii) Fig. 13 and Fig. 14 correspond to the peripheral zones at

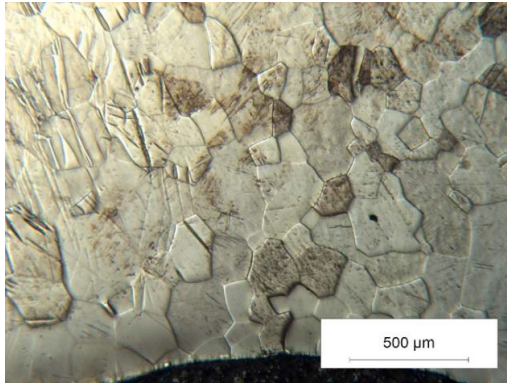


Fig. 16. Upper zone for a large length ($d = 4$ mm).

In the upper zones, there is practically no twinning in many grains (right side of the figures). In other grains, twinning is active but to a lesser extent compared to the activation at the tips of the hollow shapes after plastic deformation (Fig. 11 to Fig. 14). In the figures, activation of twinning becomes most important in the upper areas when the observation is performed towards the central zones.

The results of this part of the study indicate specific variations which can contribute to the differences measured on the experimental force-displacement curves. For instance, a comparison of the geometries of the tips of the new hollow shapes in the peripheral zones (Fig. 13 and Fig. 14) indicates the specificity of geometric contributions to the mechanical response. Moreover, the activation of the deformation modes and notably of twinning may also depend on the geometry of the sample. For instance, the central zones of Fig. 11 and Fig. 12 may have specific deformation stages. The activation of this mechanism of deformation in neighbouring grains is presented in the following section.

3.4. EBSD analysis between new hollow shapes

The microstructure after the mechanical tests is analyzed in this section with the EBSD technique for two particular cases. The objectives in the first case are (i) the determination and the characterization of the crystallographic orientations of the twinned and non-twinned parts of grains for a large area between two new hollow shapes. In addition, for this first particular case, the other objective is (ii) to determine and to characterize the local crystallographic texture by the presentation of pole figures ($\{0002\}$ and $\{10\bar{1}0\}$ poles). Then, a large zone is considered in order to take into account numerous grains. For this first case, the specimen associated with $d = 4$ mm is chosen. Indeed, the large map corresponds to a measurement area of $2000 \mu\text{m} \times 2000 \mu\text{m}$ with an acquisition step of $3.5 \mu\text{m}$ during the EBSD scans. In the second particular case, the main objectives are (i) to provide an example with a particular interesting view of activation of twinning with fine details of this deformation mode and (ii) to identify few twins in this particular example. Then, a smallest map associated with $d = 1$ mm has been found and chosen for the observation and the characterization. It corresponds to a map of $240 \mu\text{m} \times 180 \mu\text{m}$ area with a finer step of $0.8 \mu\text{m}$. At the stage of the present

study, a large EBSD map (of $2000 \mu\text{m} \times 2000 \mu\text{m}$) is considered only for one specimen ($d = 4$ mm) and a finer map (of the order of $240 \mu\text{m} \times 180 \mu\text{m}$) is considered only for the specimen mentioned above ($d = 1$ mm).

The experimental acquisitions associated with $d = 4$ mm are presented in Fig. 17, Fig. 18 and Fig. 19. The colors of the maps indicate inverse pole figures (IPF) for the ND_0 and TD_0 directions respectively. The horizontal and vertical directions of the figures correspond respectively to RD_0 and ND_0 . These maps are particularly interesting since they show the local shapes and orientations of grains in the same neighborhoods. The colors of the IPF associated with ND_0 and TD_0 indicate that the majority of the grains with twinning have the c-axis of the hexagonal cell in the vicinity of the compression direction, that is to say close to ND_0 in the study. The twinned parts have their c-axis in positions close the plane defined by the TD_0 and RD_0 directions.

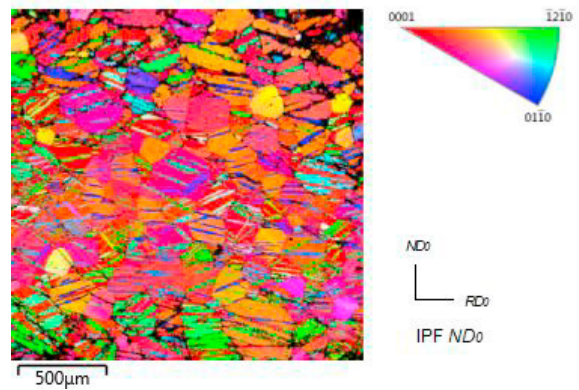


Fig. 17. EBSD map for a large length: IPF of ND_0 ($d = 4$ mm).

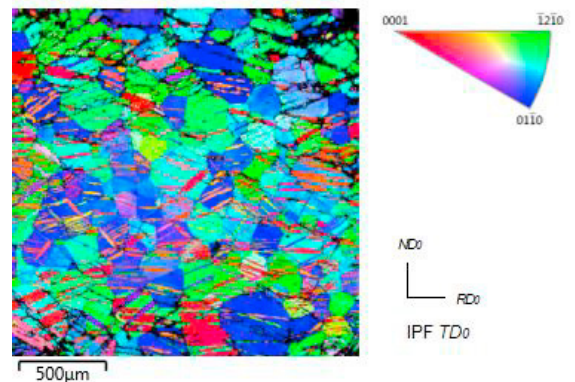


Fig. 18. EBSD map for a large length: IPF of TD_0 ($d = 4$ mm).

Concerning the crystallographic texture after plastic deformation, the $\{0002\}$ and $\{10\bar{1}0\}$ pole figures associated with the large central area of $2000 \mu\text{m} \times 2000 \mu\text{m}$ of Fig. 17 and Fig. 18 are presented in Fig. 19. Two maxima are determined near the (ND_0-TD_0) plane for the basal poles $\{0002\}$. The majority of these poles is gathered in the vicinity of the normal direction ND_0 . The main intensities of the prismatic poles $\{10\bar{1}0\}$ are found near the (TD_0-RD_0) plane.

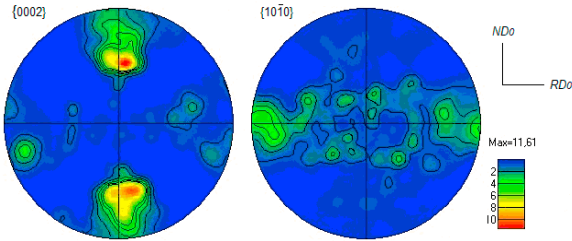


Fig. 19. Pole figures of the central zone for a large length ($d = 4$ mm).

The microstructure of Fig. 20 presents the fine details of the activation of twinning in the selected zone. In the bottom of the micrograph, twins are visible inside other twins. For the identification of the type of a twin, the misorientation between the parent grain and the twinned part of a grain can be determined. This misorientation is defined by a rotation angle of the c-axis of the parent grain and a crystallographic axis of rotation [21,17]. In titanium, for the extension twins of $\{10\bar{1}2\}\langle 10\bar{1}\bar{1}\rangle$ type, this angle equals 85.0° and for contraction twins of $\{11\bar{2}2\}\langle 11\bar{2}\bar{3}\rangle$ type this angle equals 64.4° [21,17]. The misorientation profile (point-to-point profile) of segment AB indicated in Fig. 20 is presented in Fig. 21. This type of profile has been used in the literature for identification of twinning in commercially pure titanium [17]. In Fig. 21, the identified misorientation angles are close to the theoretical value 64.4° associated with $\{11\bar{2}2\}\langle 11\bar{2}\bar{3}\rangle$ twinning.

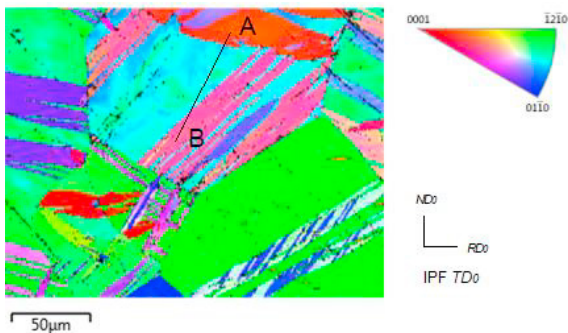


Fig. 20. EBSD characterization of twinning ($d = 1$ mm).

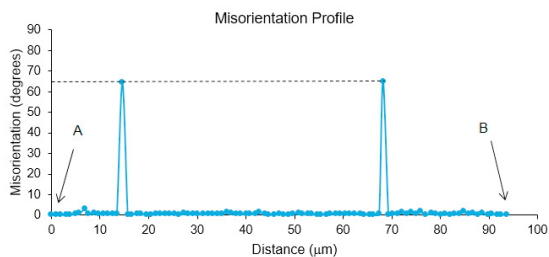


Fig. 21. EBSD point-to-point profile ($d = 1$ mm), along A-B Fig. 20.

The experimental results and their analysis indicate that there are significant differences between the investigated

specimens according to the experimental values of d . The force-displacement curves show specific evolutions. The geometry of the specimens after the mechanical tests indicate also variations at the macroscale and at the scale of the vicinity of the new hollow shapes. The analysis of the microstructures of the deformed specimens and the determination of local crystallographic orientations with the EBSD technique of neighboring grains show the importance of the activation of twinning in the analyzed specimens.

4. Conclusion

Specimens of commercially pure titanium with a specific geometry have been deformed at room temperature according to an experimental protocol. The specimens were initially defined by a characteristic length noted d between two hollow shapes. Four values of d have been investigated : 1 mm, 2 mm, 3 mm and 4 mm. The specimens were deformed using the device of a compression machine. The following conclusions can be drawn. (i) The force-displacement curves indicate that the force levels present significant differences : for a fixed value of the displacement, the force level increases when d increases. In addition, the shapes of the experimental force-displacement curves are not rigorously the same and evolve with d . (ii) The geometry of the external surfaces indicates an increase of the maximal length noted L when d increases. Moreover, the curvature of these external surfaces presents different profiles notably for $d = 1$ mm and $d = 4$ mm. Moreover, concerning the new hollow shapes after the mechanical tests, the experimental values indicate significant evolutions for the relative distance variations associated with b and d^* , versus d . (iii) Different degrees of activation of twinning are determined in the vicinity of the central, peripheral and upper zones of the new hollow shapes of the specimens. The correlations between the geometric changes of the specimens and the local plastic deformations due to the active deformation modes are not direct. They need to consider specific mechanical models to provide satisfying descriptions. (iv) Local crystallographic orientations have been determined between new hollow shapes thanks the EBSD technique. For most of the grains, activation of twinning corresponds to grains with c-axes close to the normal direction of the specimen. Most of the twinned parts of the grains correspond to orientations with c-axes close to the transverse - longitudinal plane. $\{11\bar{2}2\}\langle 11\bar{2}\bar{3}\rangle$ compression twinning has been identified. (v) The procedure used in the study gains access to experimental data related to the effects of the characteristic length d between the initial hollow shapes and related to the selected mechanical process of deformation. The data are useful quantities for calculations using the finite element method.

References

- [1] Amouzou KEK, Richeton T, Roth A, Lebyodkin MA, Lebedkina TA. Micromechanical modeling of hardening mechanisms in commercially pure α -titanium in tensile condition. *Int J of Plast* 2016;80:222–40.
- [2] Kahn AS, Kazmi R, Farrokh B, Zupan M. Effect of oxygen content and microstructure on the thermo mechanical response of three Ti-6Al-4V alloys: Experiments and modeling over a wide range of strain-rates and temperatures. *Int J of Plast* 2007;23:1105–25.

- [3] Francillette H, Benmaouche M, Gauquelin N. Anisotropic behavior of a Ti-6Al-4V sheet during cold rolling : Evidence of macroscopic shearing. *J of Mater Process Techn* 2008;198:86-92.
- [4] Francillette H, Garand C. Formability and macroscopic shearing of a titanium alloy Ti-6Al-4V under channel die compression. *AIP Conference Proceeding* 2017;1896:020005. American Institute of Physics. doi.org/10.1063/1.5007962.
- [5] Xu F, Holt RA, Daymond MR, Rogge RB, Oliver EC. Development of internal strains in textured Zircaloy-2 during uni-axial deformation. *Mater Sci Eng A* 2008;488:172-85.
- [6] Francillette H, Bacroix B, Gaspérini M, Béchade JL. Effect of initial textures on deformation mechanisms and texture evolutions of Zr α polycrystals deformed by channel die compression tests. *Mater Sci Eng A* 1997;234:974-7.
- [7] Francillette H, Bacroix B, Gaspérini M, Béchade JL. Grain orientation effects in Zr702 α polycrystalline samples deformed in channel die compression at room temperature. *Acta Mater* 1998;46:4131-42.
- [8] Biswas S, Kim DI, Suwas S. Asymmetric and symmetric rolling of magnesium : Evolution of microstructure, texture and mechanical properties. *Mater Sci Eng A* 2012;550:19-30.
- [9] Francillette H, Marco F. Formability of a magnesium alloy AZ31B deformed under channel die compression tests : macroscopic shearing of specimens. *Key Eng Mater* 2015;651-653:15-20.
- [10] Schlosser F, Signorelli J, Leonard M, Roatta A, Milesi M, Bozzolo N. Influence of the strain path changes on the formability of a zinc sheet. *J of Mater Process Techn* 2019;271:101-10.
- [11] Boyer RR. An overview on the use of titanium in the aerospace industry. *Mater Sci Eng A* 1996;213:103-14.
- [12] Gunderov DV, Polyakov AV, Semenova IP, Raab GI, Churakova AA, Gimaltdinova EI, Sabirov I, Segurado J, Sitdikov VD, Alexandrov IV, Enikeev NA, Valiev RZ. Evolution of microstructure, macrotexture and mechanical properties of commercially pure Ti during ECAP-conform processing and drawing. *Mater Sci Eng A* 2013;562:128-36.
- [13] Benmhenni N, Bouvier S, Brenner R, Chauveau T, Bacroix B. Micromechanical modelling of monotonic loading of CP- α Ti: Correlation between macroscopic and microscopic behaviour. *Mater Sci Eng A* 2013;573:222-33.
- [14] Wronski S, Wierzbowski K, Jedrychowski M, Tarasiuk J, Wronski M, Baczanski A, Bacroix B. Microstructure evolution of titanium after tensile test. *Mater Sci Eng A* 2016;656:1-11.
- [15] Bishoyi BD, Sabat RK, Sahoo SK. Effect of temperature on microstructure, texture evolutions during uniaxial compression of commercially pure titanium. *Mater Sci Eng A* 2018;718:398-411.
- [16] Chun YB, Yu SH, Semiati SL, Hwang SK. Effect of deformation twinning on microstructure and texture evolution during cold rolling of CP-titanium. *Mater Sci. Eng A* 2005;398:209-19.
- [17] Bouvier S, Benmhenni N, Tirry W, Gregory F, Nixon ME, Cazacu O, Rabet L. Hardening in relation with microstructure evolution of high purity α -titanium deformed under monotonic and cyclic simple shear loadings at room temperature. *Mater Sci Eng A* 2012;535:12-21.
- [18] Stolyarov VV, Zhu YT, Alexandrov IV, Lowe TC, Valiev RZ. Influence of ECAP routes on the microstructure and properties of pure Ti. *Mater Sci Eng A* 2001;299:59-67.
- [19] Islimgaliev RK, Kazyhanov VU, Shestakova LO, Sharafutdinov AV, Valiev RZ. Microstructure and mechanical properties of titanium (Grade 4) processed by high-pressure torsion. *Mater Sci Eng A* 2008;493:190-4.
- [20] Becker H, Pantleon W. Work-hardening stages and deformation mechanism maps during tensile deformation of commercially pure titanium. *Comput Mater Sci* 2013;76:52-9.
- [21] Song SG, Gray III GT. Structural interpretation of the nucleation and growth of deformation twins in Zr and Ti - I. Application of the coincidence site lattice (csl) theory to twinning problems in HCP structures. *Acta Metall Mater* 1995;43:2325-37.